

# Spray freeze drying of YSZ nanopowder

Bala P. C. Raghupathy · J. G. P. Binner

Received: 5 October 2011 / Accepted: 10 May 2012  
© Springer Science+Business Media B.V. 2012

**Abstract** Spray freeze drying of yttria stabilised zirconia nanopowders with a primary particle size of ~16 nm has been undertaken using different solids content starting suspensions, with the effect of the latter on the flowability and crushability of the granules being investigated. The flowability and fill density of the granules increased with an increase in the solid content of the starting suspension, whilst the crushability decreased. The powder flowability, measured using a Hall flowmeter and model shoe-die filling tests, showed that the flowability of otherwise poorly flowable nanopowders can be improved to match that of the commercial spray dried submicron powder. The 5.5 vol.% solid content based suspension yielded soft agglomerates whilst a 28 vol.% solid content suspension formed hard agglomerates on spray freeze drying; the granule relics were visible in the fracture surface of the die pressed green compact in the latter case. The increase in granule strength is

explained by the reduction in inter-particle distance based on the theories developed by Rumpf and Kendall. The flaw sizes computed using the Kendall model are comparable with those seen in the micrographs of the granule. With an optimum solid content, it is possible to have a granulated nanopowder with reasonable flowability and compactability resulting in homogeneous green bodies with ~54 % of theoretical density.

**Keywords** YSZ · Spray freeze drying · Agglomerate strength · Powder flowability · Die pressing · Nitrogen adsorption isotherms · Nanostructured ceramics

## Introduction

Spray freeze drying (SFDing), also known as lyophilisation, is widely used in the pharmaceutical and food industries for drying temperature sensitive materials. When used for ceramic materials, it offers control over the particle shape and generally results in softer granules compared to the more commonly used spray drying (SDing) and so forms an homogeneous green body on compaction (Amato et al. 1976; Tallón et al. 2006; Moritz and Nagy 2002; Uchida et al. 2002); this is potentially very useful for processing nanoceramic powders. The commercial exploitation and mass manufacture of nanostructured ceramics will require the continuous and reliable production of components in high volumes. Since die pressing is the most widely

---

**Electronic supplementary material** The online version of this article (doi:10.1007/s11051-012-0921-6) contains supplementary material, which is available to authorized users.

---

B. P. C. Raghupathy (✉)  
Center for Nanotechnology Research,  
VIT University, Vellore, India  
e-mail: balapraveen2000@yahoo.com

J. G. P. Binner  
Department of Materials, Loughborough University,  
Loughborough, UK

used existing ceramic fabrication technique, high and consistent flowability and crushability are of paramount importance; these will necessitate controlled granulation where the granules flow well but crush easily (Raghupathy and Binner 2011). Hence, it is envisaged (Chen and Wang 2007) that the granulation of nanomaterials via SFDing will be a standard process route in the future. Amongst the various ceramic materials, yttria stabilized zirconia is technologically important for its wide range of applications from solid oxide fuel cells to artificial hip joints, metal drawing dies to petroleum valve liners.

To the best of the authors' knowledge, all previous work on the SFDing of ceramic powders has resulted in low density granules. SFDing, and its related process route freeze casting, do not involve the capillary forces that are common in SDing and slip casting (Moritz and Nagy 2004). As a result, there is a direct dependence between the initial solid loading of the suspension and the resultant porosity of the SFD granules, i.e. a high solid content suspension leads to a high granule density. The latter, in turn, generally lead to high green density bodies after compaction, a desirable result. However, high density granules cannot be prepared unless the precursor high solid content suspension has a low enough viscosity to permit spraying. This is a challenge since the viscosity of nanosuspensions increases sharply with solid content (Li and Akinc 2005). However, it has been achieved for an yttria stabilized zirconia nanosuspension via use of appropriate dispersants, pH control and ultrasonication with viscosities of  $\sim 0.2$  Pa s being retained whilst achieving solids contents of up to  $\sim 34$  vol.% (Binner et al. 2006). This suspension been used as the precursor in the present study.

Further, again to the best of our knowledge, this is the first attempt to verify Kendall's theory of agglomerate strength (Kendall 1988) for granules made of nanoceramic powders. To date, we believe that the theory has only previously been examined for submicron ceramic powders (Park et al. 1993; Antonyuk et al. 2005) and pharmaceutical particles (Adi et al. 2011). Njiwa et al. (2006) studied the mechanical properties of dry pressed nanocrystalline alumina powder compacts and rationalized the high fracture toughness of green compacts to the contact flattening between particles. The breakage behaviour of various powder granules with submicron primary particles of  $\gamma$ -alumina, zeolite and sodium benzoate was studied

and reported (Antonyuk et al. 2005). Barekar et al. (2009) used Kendall's model to assess the strength of the micron sized agglomerates of silicon carbide. In this study, the measured single granule strengths correlate well with the theoretical prediction and give critical flaw size values close to those observed using electron microscopy.

## Experimental procedure

A well dispersed suspension of 3 mol% yttria stabilised zirconia (3YSZ) with an average particle size of  $\sim 16$  nm was supplied by MEL Chemicals, UK. It had a solid content of 5.5 vol.% (26 wt%) in water and no other additives. The pH varied slightly between batches but was always between 2 and 3. The suspensions were concentrated using a route described elsewhere (Santacruz et al. 2008) but which essentially involved changing the suspension pH to a value of  $\sim 10$  using tetra-methyl ammonium hydroxide, TMAH, (Aldrich Chemicals Ltd., Dorset, UK) and then adding  $\sim 2.5$  wt% tri-ammonium citrate, TAC (FSA Laboratory, Loughborough, UK). The suspension was subsequently heated at  $60$  °C in a water bath until the solid content of the suspension reached  $>14.3$  vol.% (50 wt%) and at appropriate intervals (Binner et al. 2006) it was exposed to ultrasonics (Soniprep 150, MSE Scientific Instruments, Manchester, UK; ultrasonic frequency 23 kHz; maximum power 150 W; amplitude  $12$   $\mu$ m) to break down any agglomerates present between the primary particles. Throughout the concentration process, the suspension was kept under vigorous stirring to maintain homogeneity. The viscosity of the suspension was required to be lower than 1 Pa s to be able to spray the suspension.

The zeta-potential of the suspensions was measured using an Acoustosizer II (Colloidal Dynamics, Sydney, Australia). Suspension flow behaviour was monitored using a Bohlin Visco 88 viscometer (Bohlin Instruments UK, Cirencester, UK), a controlled speed device that measures shear stress and viscosity as a function of shear rate. Measurements were recorded in a sweep cycle of continuous increasing and then decreasing shear rate ranging from 56 to  $1,000$   $s^{-1}$ .

SDing of the as-received nanosuspension was performed using a spray dryer (Production Minor, GEA Niro, Copenhagen, Denmark) with a rotary atomiser with the inlet and outlet stream temperatures

maintained at 210 and 120 °C, respectively. For SFDing, ultrasonic atomisation was used to spray the nanosuspensions onto liquid nitrogen. The suspension was slowly delivered on a vibrating ultrasonic horn using a plastic pipette; the ultrasonic frequency was 23 kHz and the amplitude was maintained at 12 μm. The fine droplets thus created were collected in a beaker filled with liquid nitrogen, converting them into frozen granules instantaneously. At the end of the process, the excess nitrogen was evaporated off and the frozen granules were dried by sublimation in a benchtop freeze dryer (Virtis benchtop SLC, New York, USA) at less than 240 K under a vacuum of ~0.2 mbar. A submicron powder (TZ-3YSB-C, Tosoh Corporation, Tokyo, Japan) was used for benchmarking the granulated nanopowders and used as-received. The codes for the different powders used are given in Table 1.

Powder X-ray diffraction, XRD (Bruker AXS D8 Advances, Karlsruhe, Germany), was used to identify the crystallite phases. The scanning rate was 2° 2θ per minute and CuKα radiation with a wavelength of 1.5406 nm was used. The lattice spacing, *d*, was calculated using Bragg’s law:

$$n\lambda = 2d \sin \theta_B \tag{1}$$

where *n* is an integer, λ is the wavelength of X-ray source and θ<sub>B</sub> is the angle between the incident ray and scattering plane.

X-ray line broadening was used to find the crystallite size (Boulch et al. 2001) assuming that the crystals were free of strains or faulting, the crystallite size was found using the Scherrer formula:

$$L = (0.9\lambda)/(\theta * \cos \theta_B) \tag{2}$$

where *L* is the crystallite domain size in nm, λ the wavelength in nm, θ the full width at half maximum, FWHM, in radians, and θ<sub>B</sub> the Bragg diffraction angle in degrees. *L* is considered as an average crystal dimension perpendicular to the reflecting planes.

The powder flowability was measured using a Hall flowmeter for freely flowing powders (Lukasiewicz 1989; Tan 2004). The powder flow rate was assessed using three different orifice diameters, viz. 2.5, 5 and 7.5 mm. The powder was poured into the funnel and collected in a density cup placed on top of a weighing balance. The microbalance had an accuracy of 0.001 g and was interfaced with a computer which recorded the mass at intervals of 0.1 s.

The powder flow was also assessed using a custom-built model shoe-die filling rig consisting of a pneumatically driven shoe, the velocity and acceleration of which could be controlled using a microprocessor. The powder was delivered to the die from the powder-filled shoe as it traversed over the fixed die cavity. A rectangular shoe of size 60 mm × 40 mm was used. The height of the powder bed was 10 mm when filled. The die opening was 14 mm × 14 mm and a constant height of 20 mm was used in all the experiments. The set-up is shown in (Wu et al. 2003) and was located at Leicester University, UK.

The shoe acceleration was fixed at 50 m s<sup>-2</sup> and the weight of the powder in the die was noted for seven different shoe speeds, viz. 50, 100, 150, 200, 300, 500 and 750 mm s<sup>-1</sup>. The shoe was programed to have five quick shakes of ±5 mm before it was translated once over the die. The shakes were designed to nullify any effects arising from filling the shoe manually and aid in achieving a reproducible initial state for the powder inside the shoe. The shoe velocity profile for the die filling is pictorially depicted in Fig. 1. This profile had an initial acceleration period, (0 – *t<sub>a</sub>*), where the shoe started from rest and reached a steady-state velocity, *V<sub>shoe</sub>*, as programed; the shoe continued to travel at the predefined speed until it reached the other side of the die and started decelerating at time *t<sub>d</sub>*. Finally, at time *t<sub>f</sub>*, the entire operation was completed and the shoe came to rest.

The shoe and the die were all made of transparent Perspex so that the whole process could be captured using a high-speed camera and qualitative comparisons made. The images were captured at 1,000 frames

**Table 1** Powder coding

Code	Precursor suspension solid content (vol.%)	Drying route
SD5	5.5	Spray drying
SFD5	5.5	Spray freeze drying
SFD14	14.3	
SFD16	16.3	
SFD20	20	
SFD21	21.4	
SFD24	24.4	
SFD28	28	
Tosoh	n/a	Spray drying

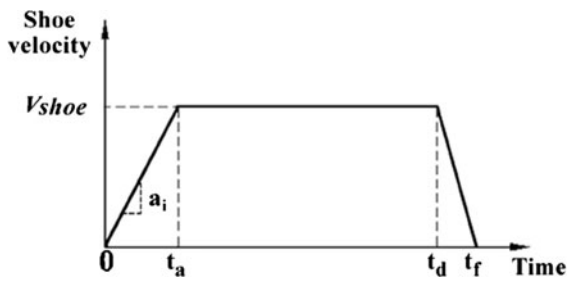


**Fig. 1** Velocity profile of the shoe used in a custom-built model shoe-die filling rig

per second using an Olympus i-SPEED high-speed digital video camera. The mass of the powder in the die after the shoe made one pass over it at the programmed velocity was measured for each of the powders to make quantitative comparisons. The powders used were SD5, SFD5, SFD14, SFD28 and Tosoh. The experimental fill ratios obtained at different shoe velocities were fitted using a power law relationship and used to deduce the critical velocity (Schneider et al. 2005).

The granule yield strength was investigated using compaction curves involving approximately 1 g of a powder for each test. The powder was filled into a 10 mm diameter die and a load was applied onto the top punch using a mechanical testing machine (L10000 Tensometer, Lloyds Instruments, Fareham, UK) with a computer interface to record the load versus cross head position continuously. The density of the compact at any given pressure was deduced from the cross head position and data on elastic compliance of the testing system at the particular load. The die and punch were cleaned thoroughly before every experiment using acetone. The maximum pressure applied was 380 MPa. Green compacts in the form of discs were also made in a uniaxial press at the same pressure. The green density of the cylindrical compacts was calculated by measuring the volume and mass of the compacts.

The crushability of individual granules was obtained using a granule strength testing system (etewe GmbH, Karlsruhe, Germany) located at the Fraunhofer Institute for Ceramic Technologies and Systems, IKTS, Dresden, Germany. The crushing force was measured for 50 granules in each batch of the powder. The diameter of each of the granules was measured automatically and crushing was done at a rate of  $10 \mu\text{m s}^{-1}$  with a separate force–displacement curve being generated for each

granule. All granules used in this study had a size within 125–250  $\mu\text{m}$ .

A transmission electron microscope (JEM 2000FX, Jeol, Tokyo, Japan) was used to examine the primary particles at high magnifications whilst the granules and the fracture surface of the green bodies were observed using a Field Emission Gun Scanning Electron Microscope (1530VP FEGSEM, Leo Elektronenmikroskopie GmbH, Oberkochen, Germany).

Nitrogen adsorption isotherms were obtained for the granules and compacts using a gas adsorption analyzer (Tristar<sup>TM</sup> 3000, Micromeritics Instrument Corporation, Norcross, USA). All powders and compacts were heated to 400 °C in air and then degassed in a nitrogen atmosphere for 30 min at 400 °C before testing. The compacts were pressed at 125 and 380 MPa to study the evolution of porosity on die pressing. The surface area was evaluated using multipoint BET method and pore size distribution using the BJH model (Barrett et al. 1951).

Finally, the nanopowder compacts that had been uniaxially pressed at 380 MPa were sintered isothermally at 1,100 °C for 1 h in a conventional furnace. The heating and the cooling rates were set at  $20 \text{ }^\circ\text{C min}^{-1}$ . The benchmark Tosoh powder was also pressed at 380 MPa, but sintered at 1,400 °C for 1 h.

## Results and discussion

### Nanosuspension characterisation

The prepared nanosuspensions were stable for at least 1 week after preparation with no sedimentation or change in rheology being observed. From Fig. 2, it is clear that the isoelectric point (IEP) shifted towards lower pH with the addition of anionic dispersants. As the pH was increased, the zeta-potential slowly decreased and the suspension flocculated when the pH reached approximately 8.3. With further pH increase the polarity of the particle charge reversed and increased in magnitude. The shift in the IEP with the addition of TAC compares well with values reported in the literature. For example, when di-ammonium citrate, a carboxylic group-containing analogue of TAC, was used the IEP was also observed to shift towards an acidic pH (Fengqiu et al. 2000). The increase in the magnitude of the zeta-potential in the high pH regime with the addition of TAC was also in line with earlier reports in

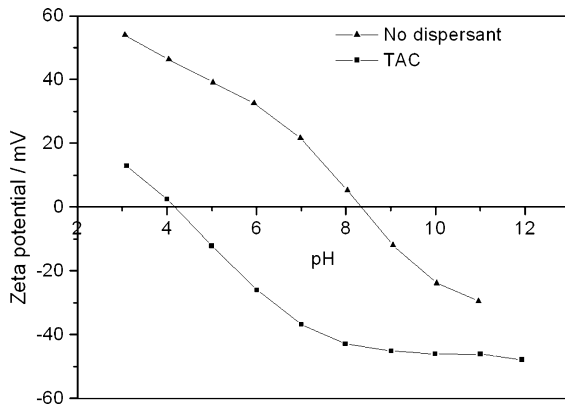


**Fig. 2** Zeta-potential for the YSZ nanosuspension before and after the addition of  $\sim 2.5$  wt% TAC

the literature (Ewais et al. 2002). Without any dispersant addition, the viscosity of the as-received nanosuspension increased sharply with an increase in solids content; at values  $>14$  vol.% it exceeded  $\sim 1$  Pa s. However, with pH control, the addition of TAC and the use of ultrasound the viscosity of nanosuspension could be kept very low,  $<0.05$  Pa s, at solid contents of at least 28 vol.%, Fig. 3. Thus, since as a rule of thumb a suspension with a zeta-potential higher than  $|30$  mV| is considered stable (Cellard et al. 2007), all the nanogranules prepared in this study were from stable and well dispersed suspensions.

The XRD patterns of the nano- and submicron powders are shown in Fig. 4a, b respectively. The peaks marked *t* correspond to the tetragonal/cubic peaks and *m* the monoclinic peaks as reported in JCPDS file 79-1769 and 78-1807, respectively. The nanopowder was completely tetragonal/cubic, as expected based on the yttria content and particle size (Garvie et al. 1975), whilst the benchmark submicron powder had both tetragonal and monoclinic peaks. The nanopowder peaks were broader in contrast to the sharper peaks of the submicron powder; the crystallite size evaluated using the Scherrer formula for the nanopowder was  $\sim 13$  nm, approximately in line with that observed experimentally using the TEM, Fig. 5. The latter also revealed that the particles were only weakly agglomerated when dispersed.

#### Granule structure

The SD5 granules were spherical, had dense packing of the primary particles and sometime had a small crater

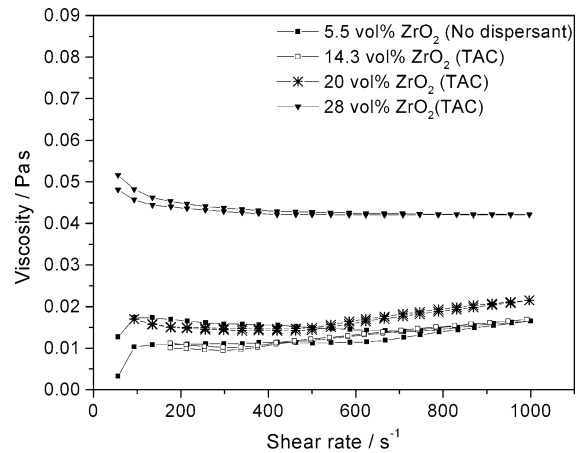


**Fig. 3** Viscosity as a function of shear rate at various solids contents and with and without the addition of  $\sim 2.5$  wt% of the dispersant TAC

or dimple, Fig. 6a. In contrast, the spherical SFD5 granules, made from the same solid content suspension, were larger and had a flaky, porous structure, Fig. 6b, the result of the absence of the very significant particle rearrangement and granule shrinkage that occurs due to capillary action during SDing. However, as the solid content of the precursor suspension was increased, the primary particles packed together more closely and hence the granule density increased, Fig. 6c–f. The benchmark, submicron Tosoh granules were generally less spherical than either of the SD or SFD nanoparticle granules and were quite often donut shaped, Fig. 6g. This is characteristic of SDing from low viscosity suspensions having high amounts of dispersants (Walker Jr. and Reed 1999; Tsetsekou et al. 2001; Mahdjoub et al. 2003; Bertrand et al. 2005). The much larger size of the primary particles in the submicron powder is also evident. Note that all of the pairs of images in Fig. 6 are shown at the same two magnifications.

#### Effect of solid content on the crushability of granules

The process of consolidating the powders into compacts was characterised using compaction curves. The increase in density with increase in pressure varied between the powders, Fig. 7. The starting point of the curve where the applied load was low approximated to the tap density of the powder. It can be seen that for the SFD nanopowders the tap density increased with

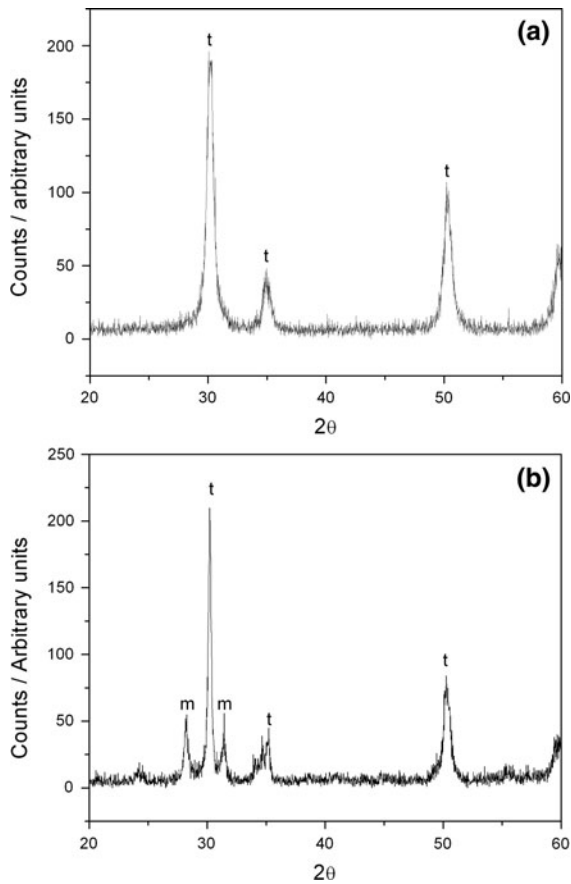


**Fig. 4** X-ray diffraction pattern for **a** the 3YSZ nanopowder and **b** the Tosoh submicron 3YSZ

increasing solid content of the precursor suspension, whilst the spray dried nanopowder and submicron benchmark powder had the highest starting densities. In each case, these results were as expected given the density of the packing of the primary particles. At low pressures, there was a little increase in density of the compact until the granules start to break; after this point, the density increased steeply with pressure. ‘Knees’ in the curve were particularly noticeable for the benchmark submicron powder and the SFD5 powder, probably as a result of the pore structure in these granules. For the rest, the crushing of the granules did not happen in a single step, but rather the granules slowly deformed as the pressure was increased. Interestingly, all of the compaction curves merged at higher pressures and reached almost the same final density, about 54–56 % of theoretical, though the Tosoh submicron and the SD5 nanopowder achieved the highest values, presumably due to their higher starting densities.

Single granule strength data confirmed the increase in the granule strength with solid content. A typical force versus deformation curve for these granules is shown in Fig. 8. Initially, the force increased proportionately with the displacement of the crushing-pin. When the elastic/plastic limit of the granule deformation was reached, the granule fractured. Immediately, the force dropped and the maximum force required for fracture was taken as the granule crushing force,  $F_C$ .

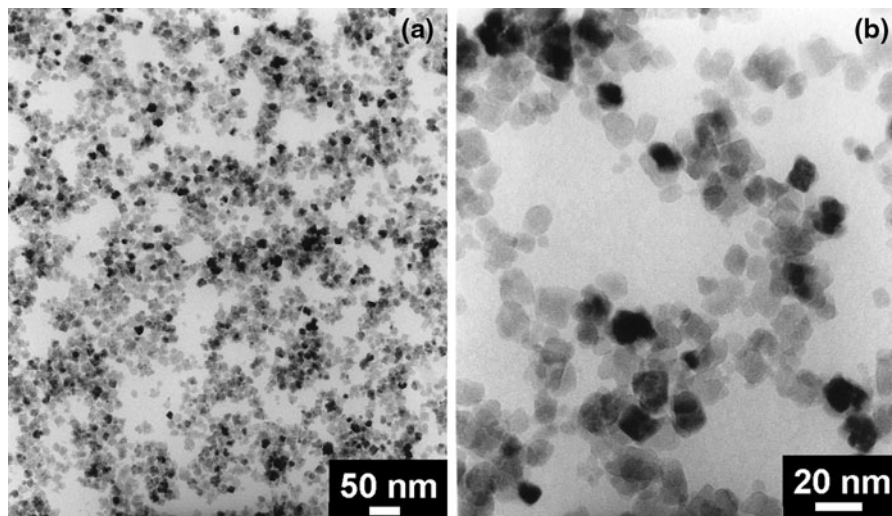


**Fig. 5** TEM image of the zirconia nanopowder at **a** low magnification and **b** high magnification showing the primary particles

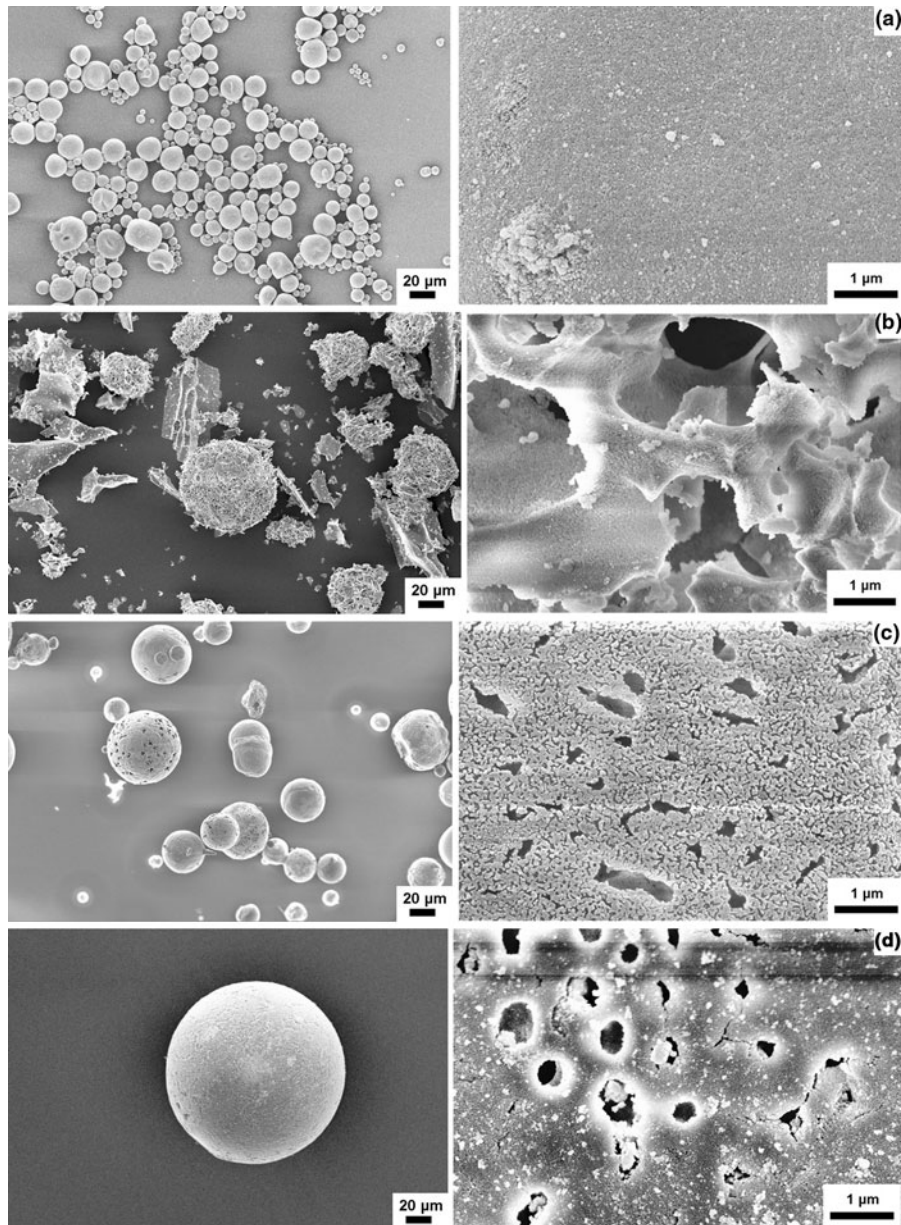


**Fig. 6** **a** SD5 granules at low and high magnification showing some drying craters and dense packing of the primary particles; **b** SFD5 granules showing a flaky and porous structure; **c** SFD14 granules showing spherical agglomerates with micro and

mesoporous structures; **d** SFD16 granules showing the sphericity of the granules and the porous surface; **e** SFD21 granules showing dense packing of the primary particles; **f** dense and spherical SFD28 granules; and **g** benchmark submicron powder from Tosoh

As the crushing-pin advanced further, the broken fragments underwent rearrangement and the force gradually increased again. The crushing force,  $F_C$ , is an important parameter to characterize the strength of the granules. For brittle fracture, the slope of the curve in the elastic–plastic deformation region should be

steep whilst ductile granules may not show a granule breaking point.

Several reasons can be envisaged for observing an increase in granule strength with increasing granule densities. First, higher granule densities imply that the particle packing is closer and hence the inter-particle

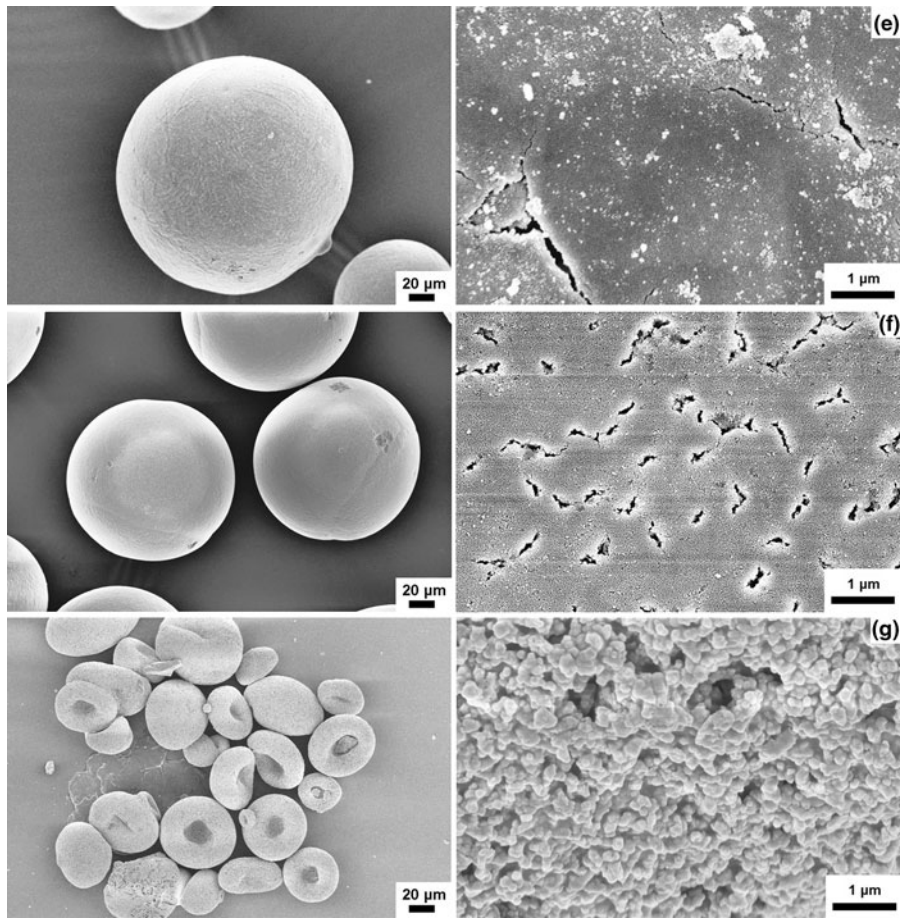


**Fig. 6** continued

distance is reduced, increasing the effect of the van der Waals forces. Second, the probability of bridging between the particles by dispersants and binders increases and, third, an increase in granule density could also reduce the effective flaw size in the granules. Two popular theories for estimating the van der Waals forces in agglomerates are by Rumpf (1962) and Kendall (Pyda and Gani 1995).

According to Rumpf's model, the normal stress  $\sigma^*$  that is applied to an agglomerate made of spherical particles of diameter  $d_p$  is distributed over all the individual inter-particle contact points (Coury and Aguiar 1995). The theory also assumes that the failure occurs simultaneously across the granule (Kendall 1988) and the limiting strength of a granule is reached when the separation force imposed by the normal

stress equals the adhesion forces. The rupture stress,  $\sigma_r^*$ , can therefore be expressed as:

$$\sigma_r^* = nF_a \quad (3)$$

where  $n$  is the average number of particle–particle contact points per unit area in the cross-section of the granule and  $F_a$  is the particle–particle adhesion force.

The parameter  $n$  is given by:

$$n = \frac{1.1(1 - \varepsilon)}{\varepsilon d_p^2} \quad (4)$$

where  $d_p$  is the diameter of the particle and  $\varepsilon$  is the agglomerate porosity. The van der Waals forces,  $F_w$ , for two dry, identical spheres of diameter  $d_p$  can be given by:

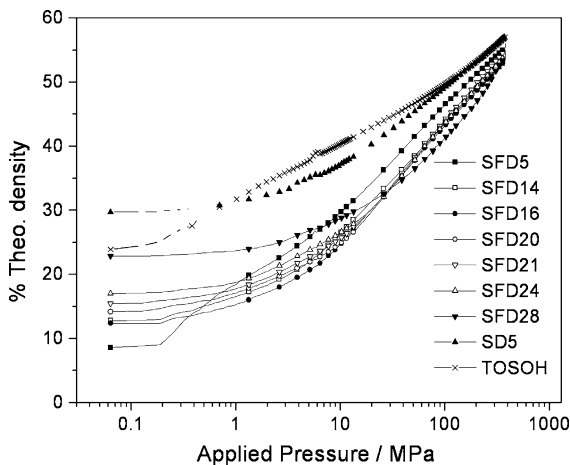


**Fig. 7** Compaction curves for the different granules

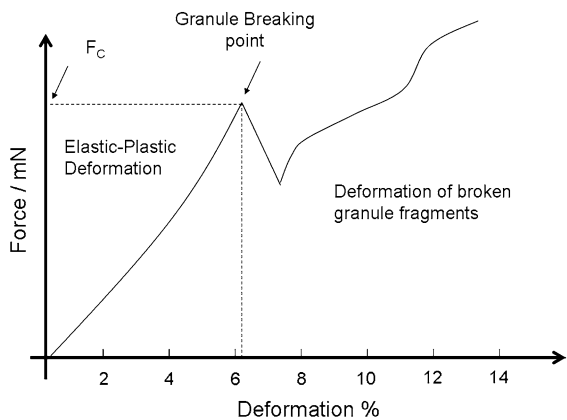


**Fig. 8** Typical granule crushing characteristics under single granule testing

$$F_w = \frac{Ad_p}{24\lambda^2} \tag{5}$$

where  $A$  is the Hamaker constant and  $\lambda$  is the separation distance between the surfaces of the particles.

Assuming that other binding forces are absent, the rupture stress can be equated to the van der Waals forces by combining Eqs. 3 and 5 as follows:

$$\sigma_r^* = \frac{nAd_p}{24\lambda^2} \tag{6}$$

Rewriting this equation yields:

$$\sigma_r^* = \frac{1.1(1 - \epsilon)A}{24\epsilon\lambda^2 d_p} \tag{7}$$

This equation was used by Song and Evans (1994) as the tensile strength of the particle assembly. As the

granule size increases, a reduction in the single granule strength has been predicted (Kendall and Weihs 1992) and demonstrated by Moritz and Nagy (2004). This is attributed to the smaller flaw sizes associated with smaller granules.

According to Kendall and Weihs (1992), the ultimate fracture strength,  $\sigma^*$ , of an agglomerate can be estimated as:

$$\sigma^* = 15.6\phi^4 \Gamma_b^{5/6} \Gamma^{1/6} (d_p c)^{-1/2} \tag{8}$$

where  $\phi$  is the volume fraction of solids in the agglomerate,  $\Gamma_b$  is the work of adhesion as measured by fracturing the contacts between the particles as opposed to the equilibrium value of adhesion energy  $\Gamma$  measured in elastic modulus tests,  $d_p$  is the primary particle size and  $c$  is the flaw size. Kendall's theory assumes a fracture mechanism similar to that of brittle materials. The effect of particle size on the work of adhesion,  $\Gamma_b$ , for nanoparticles was reported by Njiwa et al. (2006), where it increases with decreasing particle size. The  $\phi$  used in Eq. 8 is equal to  $(1 - \epsilon)$  of Eq. 7. Essentially, both theories predict that the granule strength increases with increasing granule density. As a note of caution, it must be noted that in certain cases (Adi et al. 2011) where solid bridges are formed, as in the case of drugs like mannitol, Kendall's theory may not be applicable. Recently, the conductivity of nanometric carbonaceous powder compacts were explained in relation to the particle contact area as given by Kendall (Marinho et al. 2012).

Direct experimental evidence of these theories are difficult to find owing to the difficulty in finding parameters  $\lambda$  and  $c$  for Rumpf's and Kendall's theories, respectively (Coury and Aguiar 1995). However, trends that prove the increase in granule strength with increase in granule density have been demonstrated (Moritz and Nagy 2004). The crushing force,  $F_C$ , of the different powders used in this study are shown in Fig. 9. The force required for granule fracture increases with increasing solid content of the starting suspension, i.e. granule density, as expected. From our results, it is clear that the increase in the solid content of the starting suspension not only increased the granule density, but also increased their strength after SFDing, compromising the favourable increase in flowability.

The primary zirconia nanoparticles make up granules with sizes in the range of a few microns to two

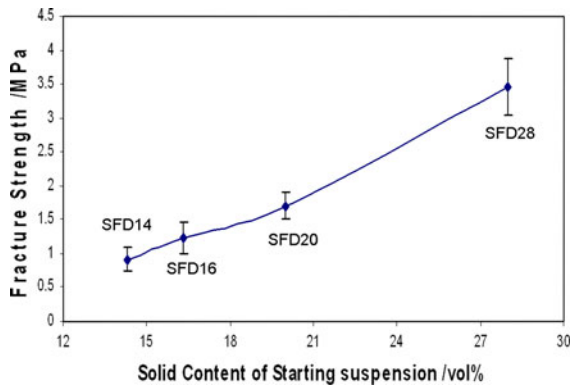


**Fig. 9** Fracture strength of granules obtained from the single granule strength tester for SFD granules from different solid content starting suspensions

hundred microns. Consider for example, a typical 150  $\mu\text{m}$  granule. Depending on the porosity of the granule, the number of primary particles would range from  $\sim 5.3 \times 10^9$  to  $\sim 2.1 \times 10^{10}$  for porosities of 90 and 60 %, respectively. The interparticle distance within the granules has been calculated assuming simple cubic packing, Table 2. The reduction in separation distance increases the short range van der Waals forces as per Rumpf's model. Substituting these values into Eq. 5, it can be inferred that the rupture stress will be  $\sim 175$  times and  $\sim 13$  times higher for SFD granules from 28 to 14.3 vol.% solids based suspensions as compared to a granule from the 5.5 vol.% solids suspension. Whilst these theoretical values based in Rumpf's theory gave a feel for the important role played by granule density, they do not agree well with the experimentally observed results suggesting that there may be more factors to consider.

In order to verify if Kendall's model would give a better fit, the theoretical value obtained for each different solids content was compared with that of the relevant experimentally measured average granule strength from the measurement system at the IKTS in Dresden. The values of  $\Gamma_b$  and  $\Gamma$  were taken as 34.5 and  $0.3 \text{ J m}^{-2}$  (Kendall and Weihs 1992), respectively. From Table 2 it can be noted that the obtained value of flaw size ranges from  $\sim 0.6$  to  $10 \mu\text{m}$ , which is comparable to those seen in Fig. 6. It is, however, stressed that all these values are derived from the average granule strength data, which had a Weibull modulus of typically between 2 and 4, i.e. very low, since the nature of the flaw within the granule can vary greatly during the atomization stage. For example,

the granule strength can be significantly reduced if air bubbles are incorporated into the granule. Further, slight variations in the  $\Gamma_b$  due to the presence of organic additives are ignored in these calculations.

#### Effect of solid content on the granule density

The relation between the solid content of the starting suspension and the tap density of the SFD granules is shown in Table 3. The theoretical deduction is based on the following assumptions: (i) the air inclusion during spraying was negligible, (ii) there was no shrinkage of the granules during drying, (iii) the packing efficiency of the granules was 60 % at the end of tapping and (iv) all the granules were equisized spheres. It can be seen that the experimentally obtained tap densities were higher than theoretically predicted based on the above assumptions. This was almost certainly because of the wide granule size distribution realised in practice. The calculations also broadly agree with reported experimental values for other materials in the literature (Moritz and Nagy 2004).

#### Powder flowability

The denser granules made from the higher solids content suspensions displayed a superior gravimetric flow rate, in  $\text{g s}^{-1}$ , when measured using the Hall flowmeter (Tan 2004); the mass and volumetric flow rates of the powders are presented in Fig. 10. Intermittent/poor flow was observed for the SFD granules produced from the as-received, 5.5 vol.% suspension through the 2.5 mm diameter orifice and hence the exact flow rate could not be measured. The flow rate of the SD granules from the same 5.5 vol.%  $\text{ZrO}_2$  suspension and the SFD granules from the 28 vol.% solids content suspension were both comparable to that of the benchmark Tosoh powder. Whilst flowability measurements were not carried out on SFD granules from nanosuspensions with solid content in the range 16.3–24.4 vol.% owing to limitations on the amount of powder needed for such experiments, the gravimetric flowrate of SFD14 powder was much lower than that of the Tosoh benchmark though the volumetric flowrate was comparable to it. A higher gravimetric flow corresponds to faster component manufacturability whilst a good volumetric flow rate ensures consistent flow and rearrangement in the die; only the latter was achieved with the SFD14 powders.

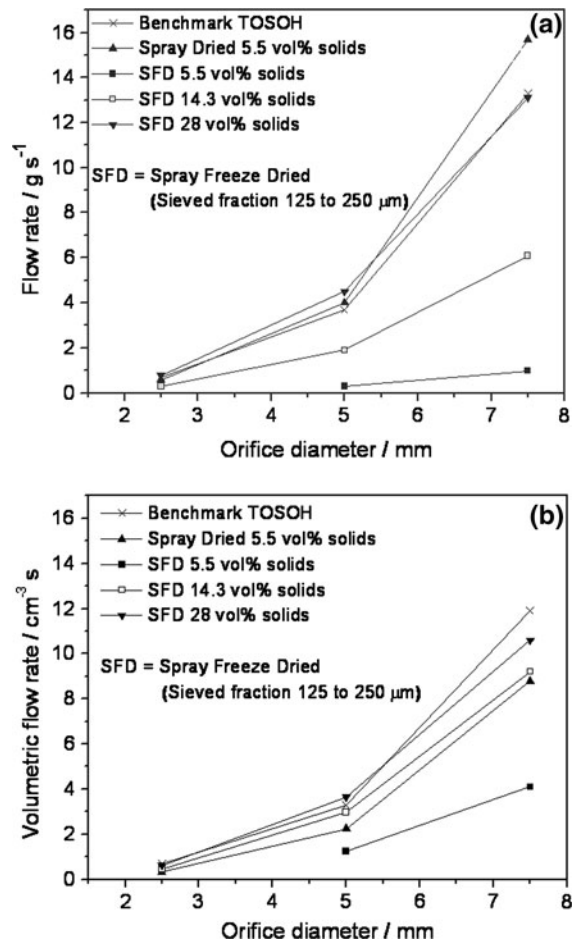
**Table 2** Relation between average inter-particle distance and starting solids content for SFD granules

Vol.% of precursor suspension	Calculated separation distance between particles, $\lambda$ (nm)	Flaw size calculated by applying Kendall's theory ( $\mu\text{m}$ )
5.5	22.8	–
14.3	10.7	0.6
16.3	9.4	1
20	7.46	2.6
28	4.5	9.4

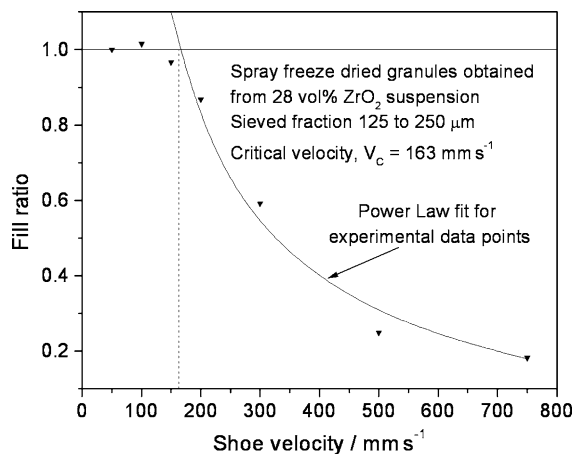
**Table 3** Theoretical and actual tap density of SFD granules

Solid content (wt%)	Solid content (vol.%)	Expected tap density ( $\text{g cm}^{-3}$ )	Expected % theoretical density	Actual tap density ( $\text{g cm}^{-3}$ )
26	5.5	0.19	3.16	0.22
50	14.3	0.51	8.57	0.65
60	20	0.72	12	–
70	28	1.00	16.8	1.24
80	40	1.44	24	–

With respect to the model die-shoe experiments, for all of the five powders tested the die was found to be completely filled when a slow shoe velocity of  $50 \text{ mm s}^{-1}$  was used. As the speed was increased, partial die filling was also increasingly observed; a typical set of data is shown in Fig. 11 for the 28 vol.% solids content nanosuspension granules. The critical velocity,  $V_C$ , is defined as the maximum shoe velocity in which the die is completely filled for a given powder and die opening and hence is a measure of the flowability of the powder; the higher the value for  $V_C$ , the better the flowability. The  $V_C$  of the various powders investigated in this study are shown in Table 4. The critical velocity of the spray freeze dried granules increased with increasing solid content of the starting suspension, a trend also observed in the Hall flowmeter. It may also be observed that the SD5 and Tosoh powders both had much lower values for  $V_C$  than the SFD 14 powder, contrary to the Hall flowmeter data. This is attributable to the granule sizes of the powders. Whilst the SFD powders measured consisted of sieved fractions with a narrow granule size distribution of 125–250  $\mu\text{m}$ , the SD5 and Tosoh powders consisted of much finer granules of  $<20$  and  $\sim 40 \mu\text{m}$ , respectively. Although, in general, powder flowability increases with increasing granule



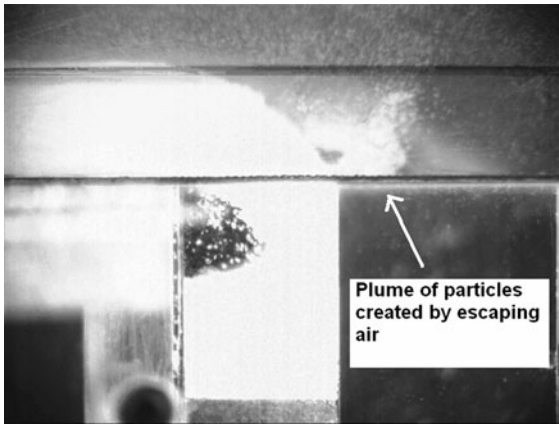
**Fig. 10** a Mass flow rate and b volumetric flow rate for the different powders through Hall flowmeters of 2.5, 5 and 7.5 mm orifice diameters



**Fig. 11** Typical die filling data for model shoe-die filling experiments showing the critical velocity,  $V_C$

**Table 4** Critical velocity of zirconia powders

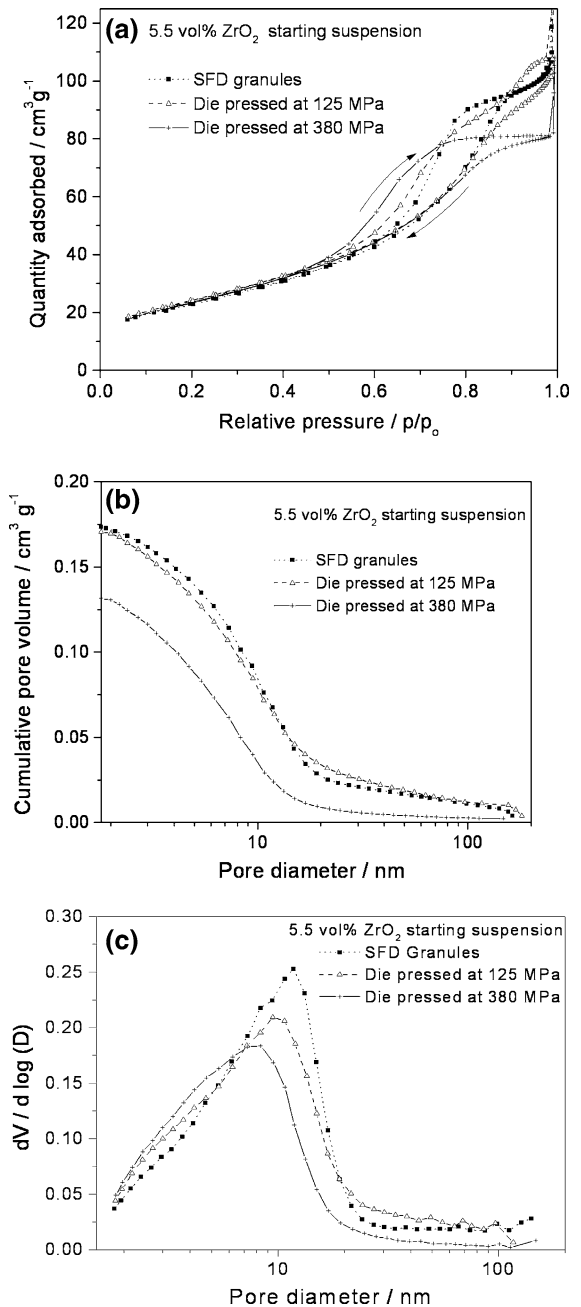
Powder	Critical velocity, $V_C$ ( $\text{mm s}^{-1}$ )
SD5	102
SFD5	86
SFD14	156
SFD28	163
Tosoh	106

**Fig. 12** Air effect in the flow pattern of SFD5 powder

density since the latter will tend to accelerate faster under the influence of gravity, and both the SD5 and Tosoh granules were the densest measured, their finer sizes meant that they were more affected by the escaping air stream (see supplementary video for details). Figure 12 shows the affect of the latter on the SFD5 powder, which had the lowest density. Similar characteristics have been explained in detail by other researchers (Schneider et al. 2005; Wu et al. 2003).

### Compact characterisation

Nitrogen adsorption isotherms are useful in characterising the fine pores, in the range 2–300 nm, in ceramic powders and compacts. Non porous powders exhibit Type II isotherms where the desorption curve retraces the adsorption curve whilst for mesoporous powders Type IV isotherms are usually observed (Gregg and Sing 1982). In the present study, Type IV isotherms were observed for all the nanopowders. This is attributed to the presence of large volumes of mesopores within the granules. These pores arise from the voids between the

**Fig. 13** **a** Nitrogen adsorption isotherm for the SFD5 powder and die pressed compacts showing a reduction in the volume of adsorbed nitrogen with an increase in density, **b** the cumulative pore size distribution and **c** the differential data showing better packing at higher consolidation pressures

nanoparticles, plus the voids created during the fast freezing stage in case of the SFD powders. The latter leads to a wide range of pores extending up to a range of

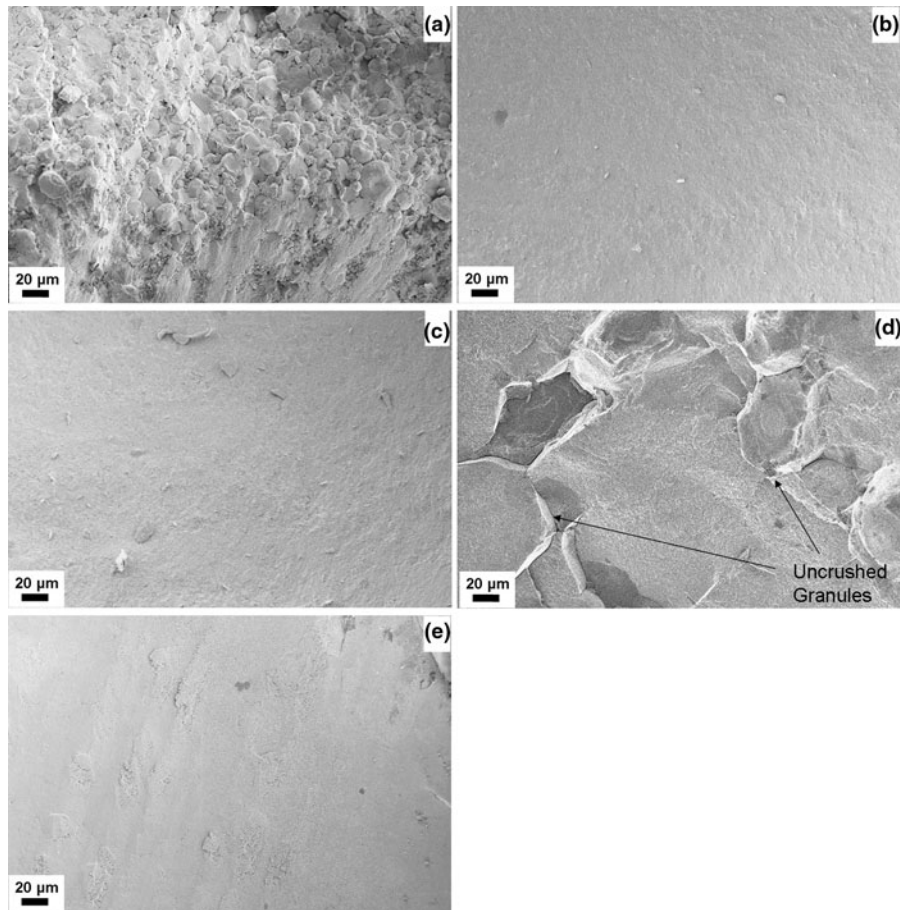


**Fig. 14** **a** Green microstructure observed from the fracture surface of an SD5 compact pressed at 380 MPa showing uncrushed granules; **b** homogeneous green microstructures observed from the fracture surface of an SFD5 compact and **c** an SFD14 compact, both pressed at 380 MPa; **d** Green

microstructure observed from the fracture surface of an SFD28 compact pressed at 380 MPa showing clear evidence of granule relics; and **e** homogeneous green microstructure observed from the fracture surface of an Tosoh compact pressed at 380 MPa

a few microns in size, as observed qualitatively in the high magnification images in Fig. 6. The reduction in porosity during the compaction stage is clearly seen in Fig. 13 for the SFD5 granules. Figure 13b shows that a consolidation pressure of 125 MPa has relatively little impact on the cumulative pore size distribution compared to the as-produced granules, whilst Fig. 13c shows the better packing achieved as the compaction pressure is increased. Similar data was seen for all the SFD granules. The increase in the hysteresis with increasing compaction pressure in Fig. 13a indicates that the pores with narrow channel openings are formed during the compaction.

The microstructure of the die pressed body from the SD5 powder can be seen in Fig. 14a. Granule relics can

be clearly seen; this is because of the high strength of the granules which did not crush, even at pressures as high as 380 MPa. On the other hand, the SFD5 and SFD14 granules crushed down completely into primary particles and yielded homogeneous fracture surfaces, Fig. 14b, c. As the solid content of the starting suspension increased further, the fracture surface of the green compacts started showing increasing signs of granule relics. The SFD28 powder was clearly the hardest of the SFD powders with the granules remaining partially uncrushed even at pressures up to 500 MPa. The uncrushed granules can be clearly seen in the compacts pressed at 380 MPa, Fig. 14d. The benchmark Tosoh powder crushed and resulted in a homogeneous green microstructure as expected, Fig. 14e.

## Conclusions

SFDing was used to produce spherical agglomerates with good flowability. These were more porous than the spray dried granules; the granule density was adjusted simply by varying the solid content of the starting suspension. The fill density and mass flow rate of the powders were directly proportional to the granule density and hence to the solid content of the starting suspension. However, due to the absence of capillary forces that shrank the granule during drying, the spray freeze dried granules had lower density than the spray dried granules.

The flowability of these powders was quantified using Hausner ratio and Hall flow and benchmarked with TOSOH submicron YSZ powder, a powder used widely in industry. With the increase in solids content of the starting suspension, the flowability of the spray freeze dried powder increased. The volumetric flow rate of the 14.3 vol.% solids based spray freeze dried powder matched with that of the benchmark. However, its gravimetric flow rate lagged behind, owing to its low granule density.

Both SDing and SFDing allowed control of the shape and size of the agglomerates, thus improving the possibility of die pressing them in an automatic industrial mass production facility. However, crushable granules with low granule strength were obtained only from SFDing. The agglomerates must be weak enough to break back down into the original nanosized primary particles when die pressed. This is important to achieve a homogeneous green microstructure that can then be sintered into fully dense nanograined ceramics without retaining uncrushed granules that could act as Griffith flaws in the final component.

The two granule properties, viz., flowability and crushability, are related to each other. With the increase in granule density, the fill ratio and flowability improved, but at the cost of crushability. The latter is of great importance if the nanostructure is to be maintained after sintering as outlined above. Hence, a trade-off between these two characteristics was sought in this case. It was found that spray freeze dried granules with 14.3 vol.% solids content worked satisfactorily, meeting both the criteria. Since industrial pressing of ceramic powders typically uses pressures of  $\leq 250$  MPa however, further work is needed to weaken the SFD granules whilst retaining their flowability. This will be the subject of future publications.

A further scientific contributions was the extension of the experimental validation of Kendall's pioneering work on granule strength to nano-sized powders. Good agreement was observed between the experimental and theoretical values of flaw size in the granules investigated meaning that nanopowder granule strength could be estimated with reasonable accuracy provided that granule density and defect size were known.

**Acknowledgments** The authors would like to thank EPSRC/PowdermatriX for financial support, Prof. Alan Cocks, Oxford University, UK, and Dr. Farhad Motazedian, Leicester University, UK, for the model shoe-die filing experiments and Mr. Nikolaos Vlachos and Prof. Issac Chang, Birmingham University, UK, for use of their Hall flowmeter. Single granule strength tests were done by Ms. Susannah Eckhard and Ms. Jing (Sherry) Liu at the Fraunhofer Institut Keramische Technologien und Systeme in Dresden, Germany, and their time and access to the equipment is gratefully acknowledged.

## References

- Adi S, Adi H, Chan H, Finlay WH, Tong Z, Yang RY (2011) Agglomerate strength and dispersion of pharmaceutical powders. *J Aerosol Sci* 42:285–294
- Amato I, Baudrocco F, Martorana D (1976) Evaluation of freeze drying and spray drying processes for preparing transparent alumina. *Mater Sci Eng* 26:73–78
- Antonyuk S, Tomas J, Heinrich S, Mörl L (2005) Breakage behaviour of spherical granulates by compression. *Chem Eng Sci* 60:4031–4044
- Barekar NS, Tzamtzis S, Hari Babu N, Fan Z, Dhindaw BK (2009) Processing of ultrafine-size particulate metal matrix composites by advanced shear technology. *Metall Mater Trans A* 40A:691–701
- Barrett EP, Joyner LG, Halenda PP (1951) The determination of pore volume and area distributions in porous substances. I. Computations from nitrogen isotherms. *J Am Chem Soc* 73:373–380
- Bertrand G, Roy P, Filiatre C, Coddet C (2005) Spray-dried ceramic powders: a quantitative correlation between slurry characteristics and shapes of the granules. *Chem Eng Sci* 60:95–102
- Binner JGP, Annapoorani K, Santacruz I (2006) Patent No. WO 2006/136780 A2, 28 Dec 2006
- Boulch F, Schouler MC, Donnadiou P, Chaix JM, Djurado E (2001) Domain size distribution of Y-TZP nano-particles using XRD and HRTEM. *Image Anal Stereol* 20:157–161
- Cellard A, Zenati R, Garnier V, Fantozzi G, Baret G (2007) Optimization of chromium oxide nanopowders dispersion for spray-drying. *J Eur Ceram Soc* 27:1017–1021
- Chen G, Wang W (2007) Role of freeze drying in nanotechnology. *Dry Technol* 25:29–35
- Coury JR, Aguiar ML (1995) Rupture of dry agglomerates. *Powder Technol* 85:37–43

- Ewais E, Zaman AA, Sigmund W (2002) Temperature induced forming of zirconia from aqueous slurries: mechanism and rheology. *J Eur Ceram Soc* 22:2805–2812
- Fengqiu T, Xiaoxian H, Yufeng Z, Jingkun G (2000) Effect of dispersants on the surface chemical properties of nano-zirconia suspensions. *Ceram Int* 26:93–97
- Garvie RC, Hannink RH, Pascoe RT (1975) Ceramic steel? *Nature* 258:703–704
- Gregg SJ, Sing KSW (1982) Adsorption, surface area and porosity, 2nd edn. Academic Press, London, pp 173–194
- Kendall K (1988) Agglomerate strength. *Powder Metall* 31: 28–31
- Kendall K, Weihs TP (1992) Adhesion of nanoparticles within spray-dried agglomerates. *J Phys D* 25:A3–A8
- Li C, Akinc M (2005) Role of bound water on the viscosity of nanometric alumina suspensions. *J Am Ceram Soc* 88: 1448–1454
- Lukasiewicz SJ (1989) Spray-drying ceramic powders. *J Am Ceram Soc* 72:617–624
- Mahdjoub H, Roy P, Filiatre C, Bertrand C, Coddet G (2003) The effect of the slurry formulation upon the morphology of spray-dried yttria stabilised zirconia particles. *J Eur Ceram Soc* 23:1637–1648
- Marinho B, Ghislandi M, Tkalya E, Koning CE, With G (2012) Electrical conductivity of compacts of graphene, multi-wall carbon nanotubes, carbon black, and graphite powder. *Powder Technol* 221:351–358
- Moritz T, Nagy A (2002) Preparation of super soft granules from nanosized ceramic powders by spray freezing. *J Nanoparticle Res* 4:439–448
- Moritz T, Nagy A (2004) Spray freeze granulates—from lab scale to pilot production presented at 7th international conference on nanostructured materials, Wiesbaden
- Njiwa ABK, Aulbach E, Rodel J (2006) Mechanical properties of dry-pressed powder compacts: case study on alumina nanoparticles. *J Am Ceram Soc* 89:2641–2644
- Park BD, Smith DM, Thoma SG (1993) Determination of agglomerate strength distributions, part 4. Analysis of multimodal particle size distributions. *Powder Technol* 76:125–133
- Pyda W, Gani MSJ (1995) Microstructural and mechanical properties of spherical zirconia-yttria granules. *J Mater Sci* 30:2121–2129
- Raghupathy BPC, Binner JGP (2011) Spray granulation of nanometric zirconia particles. *J Am Ceram Soc* 94:139–145
- Rumpf H (1962) Strength of granules and agglomerates. In: Knepper WA (ed) *Agglomeration*. Wiley-Interscience, New York, pp 379–418
- Santacruz MI, Annapoorani K, Binner JGP (2008) Preparation of high solids content nano zirconia suspensions. *J Am Ceram Soc* 91:398–405
- Schneider LCR, Cocks ACF, Apostolopoulos A (2005) Comparison of filling behaviour of metallic, ceramic, hardmetal and magnetic powders. *Powder Metall* 48:77–84
- Song J, Evans JRG (1994) A die pressing test for the estimation of agglomerate strength. *J Am Ceram Soc* 77:806–814
- Tallón C, Moreno R, Nieto MI (2006) Synthesis of  $\gamma$ - $\text{Al}_2\text{O}_3$  nanopowders by freeze-drying. *Mater Res Bull* 41: 1520–1529
- Tan O (2004) Spray drying dielectric ceramics. *Am Ceram Soc Bull* 83:12–14
- Tsetsekou A, Agrafiotis C, Leon A, Miliadis I (2001) Optimisation of the rheological properties of alumina slurries for ceramic processing applications, part II: spray drying. *J Eur Ceram Soc* 21:493–506
- Uchida N, Hiranami T, Tanaka S, Uematsu K (2002) Spray freeze dried granules for ceramics fabrication. *Am Ceram Soc Bull* 81:57–60
- Walker JS Jr, Reed WJ (1999) Influence of slurry parameters on the characteristics of spray dried granules. *J Am Ceram Soc* 82:1711–1719
- Wu CY, Dihoru L, Cocks ACF (2003) The flow of powders into simple and stepped dies. *Powder Technol* 134:24–39